Atmospheric Environment 94 (2014) 742–753

Contents lists available at ScienceDirect

Atmospheric Environment

journal homepage: www.elsevier.com/locate/atmosenv

Relationship between particulate air pollution and meteorological variables in Utah's Salt Lake Valley

C. David Whiteman*, Sebastian W. Hoch, John D. Horel, Allison Charland [1]

University of Utah, 135 S 1460 E, Rm 819, Salt Lake City, UT 84112-0110, USA

HIGHLIGHTS

- $PM_{2.5}$ is closely related to integrated atmospheric stability in the valley volume.
- No long-term trends in atmospheric stability are seen in the 40-y period of record.
- $PM_{2.5}$ rises 10 ug m^{-3} per day in multi-day episodes of high atmospheric stability.
- $PM_{2.5}$ is above the NAAQS on approximately 18 days per winter season.
- Snow cover is a key variable affecting $PM_{2.5}$ exceedances.

ARTICLE INFO

Article history:
Received 31 March 2014
Received in revised form
3 June 2014
Accepted 5 June 2014
Available online 6 June 2014

Keywords:
$PM_{2.5}$
Particulates
NAAQS exceedances
Inversions
Climatology
Salt Lake Valley

ABSTRACT

Critical meteorological factors affecting daily particulate concentrations during winter for Utah's urbanized Salt Lake Valley are examined on the basis of forty years of data. In a typical winter, the National Ambient Air Quality Standard for particulate matter with aerodynamic diameter less than 2.5 microns ($PM_{2.5}$) is exceeded during 6 multi-day events comprising 18 winter days. Multi-day episodes of high stability produce these events, as synoptic-scale high-pressure ridges transit across Utah. The *valley heat deficit*, a bulk measure of atmospheric stability, exhibits large winter-to-winter variations that are highly related to similar variations in $PM_{2.5}$. While control strategies have led to downward trends in concentrations for some primary pollutants, no long-term trends in valley heat deficit are evident over the 40 years. $PM_{2.5}$ concentrations rise gradually over a period of days after a heat deficit threshold is exceeded as the air within the valley becomes decoupled from generally stronger winds aloft. Concentrations climb at a typical rate of about 10 μg m^{-3} d^{-1} over a four-day period to about 60 μg m^{-3} during these episodes. During episodes when $PM_{2.5}$ concentrations exceed 35 μg m^{-3}, the atmospheric column in the valley is characterized by: temperature below 0 °C; relative humidity in excess of 50%; and light wind speeds. $PM_{2.5}$ concentrations in excess of 35 μg m^{-3} are four times more likely when the valley is snow covered than when it is not. A stepwise multiple linear regression based upon selected meteorological variables is used to estimate daily values of $PM_{2.5}$ during two independent winters. The correlation between observed and estimated $PM_{2.5}$ for these winters reaches 0.81.

1. Introduction

Episodes with high particulate pollution occur frequently during the winter in Utah's urbanized Salt Lake Valley (SLV) when a stable boundary layer persists for multiple days, suppressing the vertical mixing of primary aerosols and the chemical precursors that lead to secondary aerosols (Silcox et al., 2012). These stable boundary layers or persistent cold-air pools (PCAPs), which extend north and south along the west side of the Wasatch Mountains (the Wasatch Front) can continue for days, often leading to 24-h-average $PM_{2.5}$ concentrations that exceed the 35 μg m^{-3} National Ambient Air Quality Standard (NAAQS). At the northern end of the Wasatch Front in Utah's Cache Valley, for example, a 24-h-average $PM_{2.5}$ concentration reached 132.5 μg m^{-3} in an event in 2005 (Malek et al., 2006). A 4.5% increased risk of heart attacks was documented along the Wasatch Front when $PM_{2.5}$ concentrations in these long-lived events rise by 10 μg m^{-3} (Pope et al., 2006).

* Corresponding author.
E-mail address: dave.whiteman@utah.edu (C.D. Whiteman).
[1] Present address: Department of Environmental Earth Systems, Stanford University, 473 Via Ortega, Stanford, CA 94305-4216, USA.

http://dx.doi.org/10.1016/j.atmosenv.2014.06.012
1352-2310/

Emergency department visits for asthma-related illnesses increase by 42% during days 5–7 of a high pollution episode when compared to days with lower particulate concentrations (Beard et al., 2012).

The increasingly documented health effects associated with airborne particulates in these winter events (Pope et al., 1991; Peters et al., 2000), the challenges of forecasting them (Smith et al., 1997; Baker et al., 2011) and the concern that climate change might increase pollutant concentrations (Gillies et al., 2010a,b; Bailey et al., 2011; Mickley et al., 2004; Leung and Gustafson, 2005) were the impetus for the Persistent Cold-Air Pool Study (PCAPS, www.pcaps.utah.edu), a research project that focuses on improving understanding of the thermodynamical and dynamical processes associated with the persistent stable layers in the SLV during the 2010–2011 winter (Lareau et al., 2013; Lu and Zhong, 2014; Lareau and Horel, 2014a,b).

This paper provides context for PCAPS by examining relationships between meteorological conditions and particulate pollution in the SLV using atmospheric soundings and daily particulate air pollution measurements over a forty-year period. The broader objective of our study is to clarify the critical meteorological factors that control episodes of high particulate concentrations in the SLV and other similar basins and valleys that experience poor wintertime air quality.

2. Method

2.1. Measurement sites

The SLV contains the major urban area of Salt Lake City, with a population of 1,029,655 (Salt Lake County 2010 census; http://www.census.gov). The SLV has a floor elevation of about 1300 m MSL, is approximately 40 km in both width and length and is surrounded by the Wasatch Mountains to the east, the Oquirrh Mountains to the west and the Traverse Range to the south (Fig. 1). The SLV is open to the north-northwest, where the Jordan River drains into the Great Salt Lake, a large saline lake with no outlets. The confined topography of the SLV tends to shield the basin from strong external winds and trap cold air that drains into the valley from the surrounding higher terrain or intrudes into the valley with passing large-scale weather disturbances.

Twice-daily vertical profiles of temperature, moisture and wind are available from the National Weather Service at the Salt Lake International Airport (KSLC) and air quality data are available from the Utah Division of Air Quality (UDAQ) at multiple sites in the SLV (Fig. 1).

2.2. Air quality data

Air quality data from the UDAQ that are analyzed include carbon monoxide (CO) and airborne particulate matter regulated by the US Environmental Protection Agency (EPA). Particulate matter falls into three categories - total suspended particulates (TSP), particulate matter less than 10 μm in aerodynamic diameter (PM_{10}) and particulate matter less than 2.5 μm in aerodynamic diameter ($PM_{2.5}$). The primary 24-h-average NAAQS for TSP was 260 μg m^{-3} with a secondary 24-h-average standard of 150 μg m^{-3}. The size range of this sample of particulate matter was governed by the size-selectivity of the air inlet to the filter on which particles were collected. This size fraction was later found to vary depending on wind speed and direction and in 1987 the standard was superseded by a 24-h-average PM_{10} standard of 150 μg m^{-3}. In 1997, an additional 24-h-average standard was set for $PM_{2.5}$ at 65 μg m^{-3}. This standard was reduced to 35 μg m^{-3} in 2006.

Daily average data (midnight to midnight Mountain Standard Time, MST) collected by the UDAQ were obtained from the quality-controlled EPA database at www.epa.gov/ttn/airs/aqsdatamart. For CO, daily averages were formed from 1-h averages. Since measurement sites were moved during the 40-y period, we rely most heavily on the primary stations with the longest periods of record (POR) for each of the pollutants (HW for $PM_{2.5}$, NS for PM_{10}, HD for TSP, and CW for CO). When daily data are missing from the primary station, linear regression equations are used to estimate the

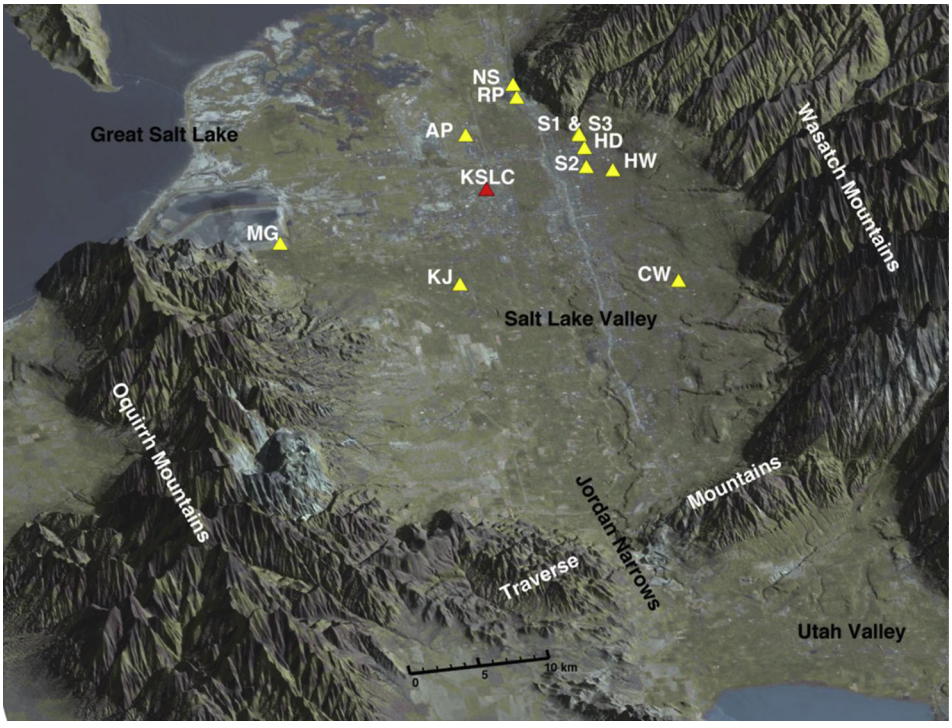

Fig. 1. Measurement sites in Utah's SLV.

missing data using relationships developed from nearby stations (Fig. 1). Detailed information on the regressions is given in the Supplemental Information.

Our analyses focused primarily on daily averages during 40 winter half-years (i.e., October through March; hereafter called winter) and on $PM_{2.5}$. The majority of $PM_{2.5}$ aerosols in the SLV are secondary aerosols produced when gases such as SO_2, NO*x* and volatile organic compounds react with other gases in the atmosphere (UDAQ, 2013). Wintertime $PM_{2.5}$ aerosols during inversion episodes in winter 2010–2011 were composed of ammonium (17%), nitrate (41%), sulfate (6%), organic carbon (19%), elemental carbon (3%), dust (3%) and other (11%) (UDAQ, 2013). A recent source attribution by Kelly et al. (2013) supports these figures, but found that secondary ammonium chloride made up 10–15% of the inventory during wintertime events when $PM_{2.5}$ exceeded 30 μg m^{-3}. Wood smoke and cooking emissions were also higher than expected from then-existing source inventories.

2.3. Meteorological data

Meteorological data come from KSLC's twice-daily rawinsonde launches and routine snow and cloud cover observations. Our analyses used 0500 and 1700 MST (1200 and 0000 UTC, respectively) soundings from 1 Jan 1973 through 31 Mar 2013. Missing or bad soundings occurred less than 3% of the time during this forty-year period. These data were obtained from a University of Wyoming archive (http://weather.uwyo.edu/upperair). For each sounding, data were interpolated to 10-m height intervals from the surface (1288 m MSL) to 5000 m MSL and vector and arithmetic wind averages and averages of other variables were then computed. Variables averaged from the surface to height *h* were designated as $\bar{\psi}_h$, where ψ represents the variable and *h* is the upper elevation bound of the average. In some analyses, the values at fixed elevations ψ_h were used directly. The following variables were extracted from the soundings: pressure *p*, temperature *T*, potential temperature θ, relative humidity *r*, wind speed *s*, wind direction *d*, east component of wind *u*, and north component of wind *v*.

Many methods have been used in the past to determine atmospheric stability from rawinsonde observations (Hosler, 1961; Holzworth and Fisher, 1979; Wolyn and McKee, 1989; Whiteman et al., 1999; Reeves and Stensrud, 2009; Gillies et al., 2010a; Zhong et al., 2011; Bailey et al., 2011; Milionis and Davies, 2008; Chen et al., 2012), with most relying on the detection of temperature inversions and requiring choices for arbitrary threshold values of lapse rates, height intervals or height ranges, and sometimes adding other wind direction or speed criteria. Stability, however, is present even when temperature inversions are absent (i.e., for temperature lapse rates between 9.8 °C km^{-1} and 0 °C km^{-1}). Inspection of soundings in the SLV showed many cases of multi-layered temperature structures with surface and elevated stable layers of different lapse rate and thickness, and ceilometer aerosol layer depths that are not necessarily constrained by major changes in vertical temperature structure (Lareau et al., 2013; Young, 2013). Thus, we use here a simplified vertically integrated approach to the calculation of valley atmospheric stability (Whiteman et al., 1999; Silcox et al., 2012; Lu and Zhong, 2014), choosing a fixed height of integration based on $PM_{2.5}$ measurements.

A bulk measure of stability in the valley termed the *heat deficit* was computed from rawinsonde soundings as

$$H_h = c_p \int_{1288\ \mathrm{m}}^{h} \rho(z)[\theta_h - \theta(z)]\mathrm{d}z \quad \left[\mathrm{J\ m^{-2}}\right] \tag{1}$$

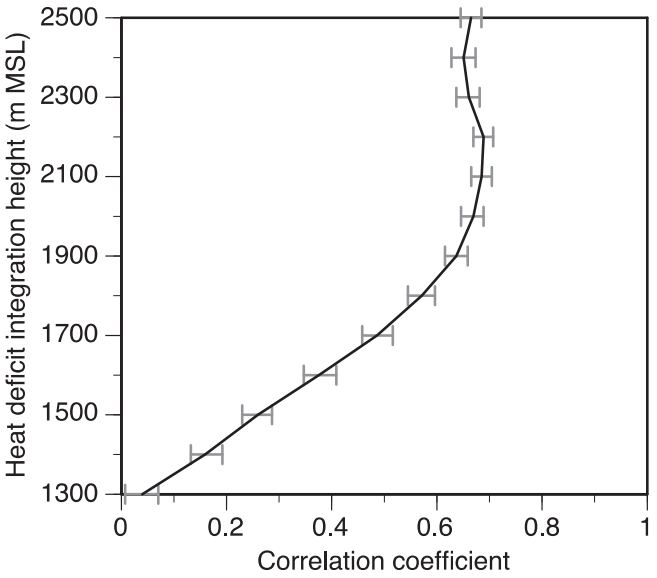

Fig. 2. $PM_{2.5}$-heat deficit correlation coefficient as a function of integration height as determined from twice-daily rawinsonde and daily $PM_{2.5}$ data for winter days from 1 Jan 1999 through 31 Dec 2011. 95% confidence intervals are determined from 1000 bootstrap replications, with replacements.

where θ_h is the potential temperature at height *h*, $\theta(z)$ and $\rho(z)$ are the potential temperature and air density from the rawinsonde sounding, $c_p = 1005$ J kg^{-1} K^{-1} is the specific heat of air at constant pressure, and *dz* is 10 m. The heat deficit is the heat required to warm an atmospheric column with a 1-m^2 base to the potential temperature at height *h*, bringing the underlying atmosphere to a dry adiabatic lapse rate. The naming convention is such that H_{22}, for example, is the heat deficit from the surface to $h = 2200$ m MSL. This method of determining bulk stability does require a choice of integration height. Because our analyses are focused mainly on $PM_{2.5}$ concentrations, we determine the integration height based on correlations between surface-based $PM_{2.5}$ measurements and the heat deficits computed to different integration heights (Fig. 2). The correlation coefficient increases strongly with height above the surface, where it reaches values near 0.65 at elevations from 2000 to 2500 m. We chose an intermediate integration height of $h = 2200$ m representative of the ridgeline elevations of the Oquirrh Mountains that define the western boundary of the valley. This is a few hundred meters below the highest peaks and is thus termed a *valley heat deficit*. By integrating (1) and using the mean air density for the winter half-year of 1.04 kg m^{-3}, the standard (ISO, 1975) and isothermal temperature lapse rates (0.0065 and 0 °C m^{-1}) are found to produce heat deficits H_{22} of 1.40 and 4.15 MJ m^{-2}, respectively.

Snow cover and low clouds and fogs are often associated with wintertime pollution episodes, as they reflect incoming solar energy back to space, reducing the available energy at the surface and thus the sensible heat flux that destroys nocturnal inversions in other seasons. The SLV often has persistent snow cover in mid-winter, and low stratiform clouds and/or fog often develop within the stable layers as moisture builds up, assisted by evaporation and sublimation from the ground and the nearby Great Salt Lake, which remains unfrozen throughout the winter. Cloud cover, snow cover, and snow depth were extracted from KSLC METAR reports. Days were considered cloudy or non-cloudy, snow covered or non-snow covered. A very conservative estimate for declaring a cloudy day was whether cloud base (broken, overcast or obscured) was present at or below 914 m (3000 ft) for both the 0500 and 1700 MST

observations. Snow cover was considered present in the valley during the entire day if present at 1700 MST. Because snow cover and snow depth generally increase with elevation within the valley and nearby mountains, data from KSLC should be considered a low estimate.

In addition to snow cover (*snoc*), cloud cover (*cldc*) and snow depth (*sdepth*), other meteorological and time variables were also investigated for relationships to air quality variables. These include maximum humidity in the *valley column* (i.e., from the surface to 2200 m MSL) r_{max}, theoretical daily total solar radiation *rad*, day of the week *dow*, and day number for episodes *doe* when H_{22} remained continuously above 4.04 MJ m^{-2}. Secondary variables included an alternate measure of stability $\theta_{22}-\theta_{sfc}$ and a Froude number

$$F_1 = \frac{\bar{s}_{22}}{\left(\frac{g}{\bar{\theta}}\frac{\partial\theta}{\partial z}\right)^{\frac{1}{2}}(h-h_0)} \cong \frac{\bar{s}_{22}}{\left(\frac{g}{c_p\bar{\rho}\bar{\theta}}H_{22}\right)^{\frac{1}{2}}} \quad (2)$$

where $\bar{s}_{22}$ is the mean wind speed from the surface to 2200 m, g is gravitational acceleration, $\bar{\theta}$ and $\bar{\rho}$ are the potential temperature and air density midway through the integration depth, h is 2200 m MSL, and h_0 is 1288 m. A second Froude number, F_2, was obtained by replacing $\bar{s}_{22}$ by s_{22}.

3. Analysis

Our goal is to determine the wintertime climatological relationships among particulate pollutants, CO, and meteorological variables in the SLV and draw conclusions that may be relevant to other basins and valleys experiencing similar air quality issues.

Time series plots for H_{22}, $PM_{2.5}$ and PM_{10} are shown for the winters of 2004–2005 and 2008–2009 in Fig. 3. Relationships among these variables are also seen in other years. First, multi-day high particulate episodes occur primarily in mid-winter. Second, $PM_{2.5}$ and PM_{10} concentrations track well, as expected, since $PM_{2.5}$ is simply a smaller size fraction of PM_{10}. Third, sawtooth-shape diurnal changes in stability on the order of 1–2 MJ m^{-2} occur in early and late winter, indicating the presence of nighttime inversions and their subsequent destruction later that day. Fourth, multi-day particulate episodes are *triggered* when the heat deficit rises above a certain threshold. Once this threshold is exceeded,

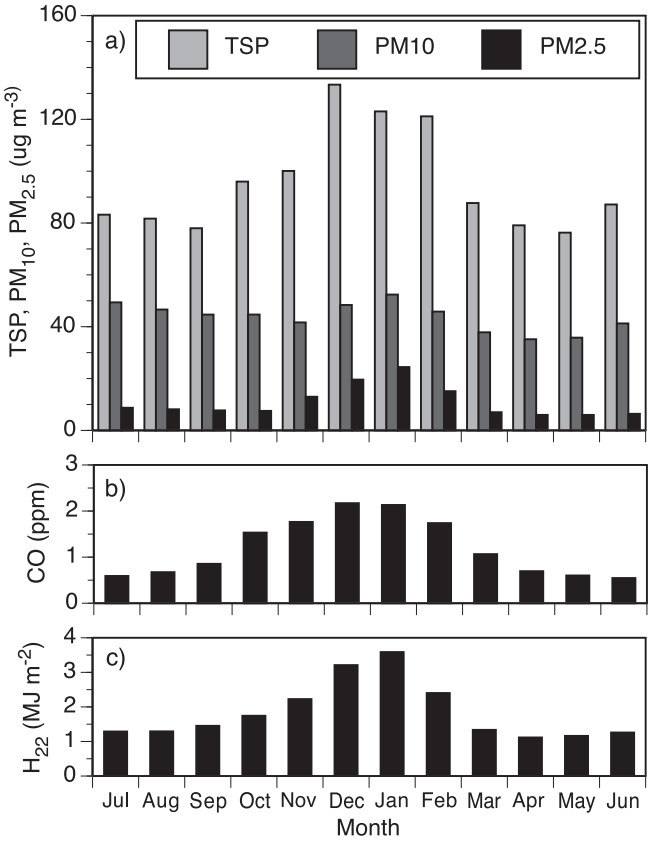

Fig. 4. Monthly means of a) daily TSP, PM_{10} and $PM_{2.5}$ concentrations, b) daily CO concentrations, and c) twice-daily heat deficits integrated to 2200 m MSL. PORs for TSP, PM_{10}, $PM_{2.5}$, CO and H_{22} are Jan 1970–Dec 1989, Jan 1986–Mar 2013, Jan 1999–Mar 2013, Jan 1970–Mar 2013, and Jan 1973–Mar 2013, respectively.

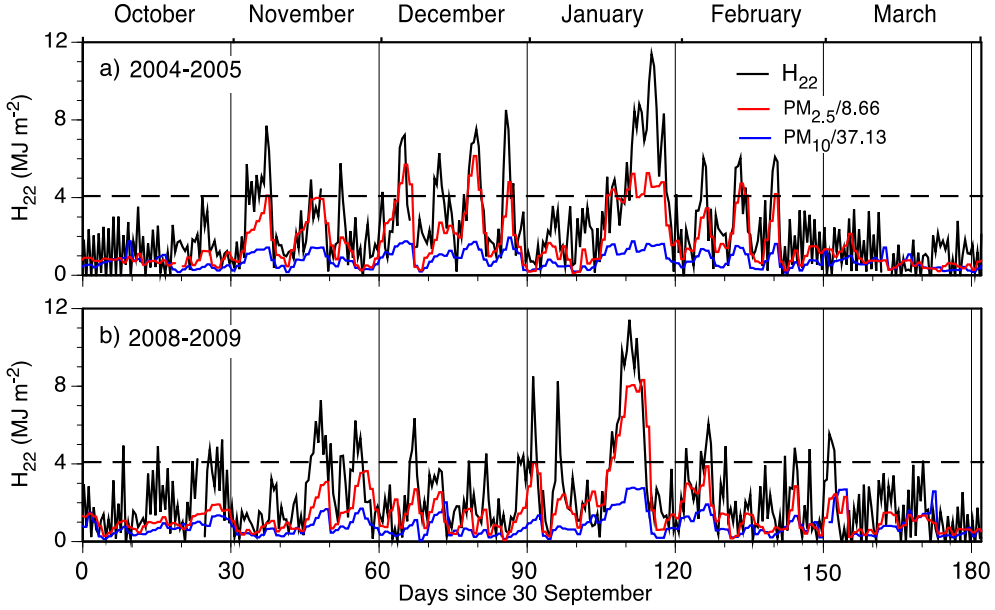

Fig. 3. Time series showing the relationships between twice-daily heat deficits H_{22} and daily PM_{10} and $PM_{2.5}$ concentrations. The dashed line marks a threshold heat deficit of 4.04 MJ m^{-2}. $PM_{2.5}$ and PM_{10} concentrations were normalized so that the dashed horizontal line also indicates the NAAQS for these variables, 35 and 150 μg m^{-3}, respectively.

$PM_{2.5}$ concentrations tend to increase monotonically from day to day, often exceeding the NAAQS. For the purposes of this paper, a reasonable threshold based on $PM_{2.5}$ concentrations and set sufficiently above the diurnal inversion signal, is the mean heat deficit (4.04 MJ m^{-2}) corresponding to all daily $PM_{2.5}$ values in the wintertime POR that exceed half of the $PM_{2.5}$ standard (i.e., 17.5 μg m^{-3}). This threshold, indicated in Fig. 3 by a horizontal dashed line, is equivalent to a constant potential temperature gradient of $d\theta/dz = 9.5$ K km^{-1} or a mean temperature lapse rate of $-dT/dz = 0.3$ °C km^{-1}. Hereafter, a series of 3 or more twice-daily soundings each having $H_{22} > 4.04$ MJ m^{-2} will be called a persistent cold-air pool or PCAP.

3.1. Air quality

Pollutant concentrations are known to vary on all temporal scales: diurnal, day-of-week, synoptic, intraseasonal, seasonal, interannual, and short- and long-term trends resulting from imposition of control strategies. We briefly summarize some of those signals in the SLV before turning in the next subsection to how meteorological factors control some of those behaviors.

Concentrations of all categories of particulate matter and CO are highest in winter (Fig. 4). For example, monthly mean $PM_{2.5}$ is highest in January (24.4 μg m^{-3}) and December (19.6 μg m^{-3}), while summer values are generally below 9 μg m^{-3}. Only three summer days exceeded $PM_{2.5}$ standards at HW since 1999; these were high wind and wildfire events. Because particulate matter exceedances are largely confined to winter, further analyses use data only from the winter half-year.

Hour-to-hour variations in emissions and photochemical processes produce a marked diurnal variation of $PM_{2.5}$ when averaged over the entire winter season POR (Fig. 5). On days when the 24-h NAAQS is exceeded, the diurnal variations are more pronounced with concentrations hovering about 35 μg m^{-3} at night and reaching a daily peak close to solar noon. CO, a relatively non-reactive gas produced largely from tailpipe emissions, has lower concentrations on the weekends than on weekdays. Weekday/weekend $PM_{2.5}$ concentrations, however, do not differ substantively (see Supplemental Information), suggesting that $PM_{2.5}$ concentrations are controlled to a large extent by chemical and photochemical reactions in the atmosphere, with reaction rates

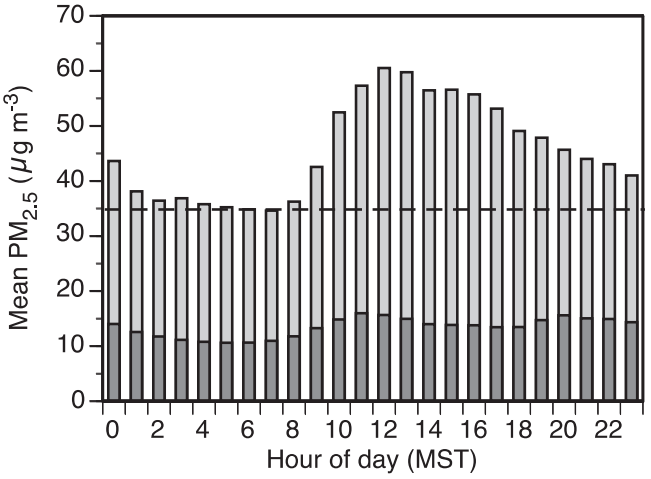

Fig. 5. Mean $PM_{2.5}$ concentration versus hour of day for winter (dark shading) and for days with 24-h-average $PM_{2.5} > 35$ (light shading). The daily NAAQS is indicated by the horizontal line. POR: 20 Feb 2009–21 Feb 2014. This POR differs from the POR for daily data, as it uses a different instrument.

such that $PM_{2.5}$ continues to be generated from precursor gases on the weekends.

The quantity of data, the number and percentage of violations of the pollutant standards, and the winter mean concentrations of the particulate pollutants and CO are presented in Fig. 6. The wintertime pollutant data sets are reasonably complete after substitutions for missing data from nearby stations (Fig. 6a). Notable exceptions include: daily TSP observations were reduced to one daily average every 6 days starting in 1982–83, with data ceasing in 1989–90; PM_{10} data was missing in the first half of the winters of 1985–86, 1992–93 and 1990–00; and $PM_{2.5}$ data began on 1 January 1999, so that data for the first half of the winter of 1998–99 are unavailable.

The numbers of winter days with concentrations above the 24-h-average NAAQS are shown in Fig. 6a and the percentage of daily wintertime observations exceeding the NAAQS are shown in Fig. 6b. The valley exceeded TSP secondary standards in the mid-seventies and early eighties, but has rarely had exceedances of the PM_{10} standard except in the late eighties and early nineties. The main continuing problem has been exceedances of the 24-h-average $PM_{2.5}$ standard, with the number varying greatly from year to year. $PM_{2.5}$ crept upward after observations were initiated and began to decrease after 2001–2002 when regulations began to take effect. The number of daily exceedances varied from 1 in 2011–12 to 32 in 2001–02. For the last 14 winters, the NAAQS has been exceeded on approximately 18 days per winter or 9.6% of the winter days.

The mean wintertime 24-h-average concentration for CO (Fig. 6c) has had a relatively consistent decline since the mid-to late-70s. In contrast, the mean wintertime concentrations of the three particulate pollutants (Fig. 6d), while declining, vary considerably from winter to winter. This variability, largely caused by intraseasonal and interannual variability in wintertime large-scale weather patterns (Gillies et al., 2010a, b), is superimposed on temporal trends that are strongly affected by the phasing of air quality regulations. Once a new NAAQS standard is promulgated, measurements made over the last several years are used to demonstrate how the non-attainment area will be brought into attainment with proposed new regulations. A State Implementation Plan (SIP) is submitted to the EPA and some time is required to get the plan approved. Pollutant emissions generally rise during this phase. Regulations are then issued to control emissions and, over a period of years, air quality improves. The temporal trends associated with this process are seen in the data for all pollutants in Fig. 6. The long-term air quality trends caused by the phasing of the regulatory process complicate climatological studies of the relationship between meteorological and air quality variables, since pollutants are controlled variables and meteorological values are random ones.

The weeks of the year having the highest $PM_{2.5}$ concentrations are shown in Fig. 7, using standardized anomalies obtained by subtracting the climatological winter mean from the climatological weekly mean of interest and dividing by the standard deviation of those weekly means. $PM_{2.5}$ standardized anomalies rise gradually during the fall and early winter, but start to fall rather precipitously in mid-February as daily solar radiation totals begin to increase rapidly and traveling storm systems become more active as spring approaches. The highest $PM_{2.5}$ standardized anomalies are found in the second and third weeks of January. PM_{10} standardized anomalies (not shown) were much more variable than for $PM_{2.5}$.

The relative frequency of different-length episodes during which the daily $PM_{2.5}$ threshold was continuously above 35 μg m^{-3} are shown in Fig. 8. The longest episode lasted 18 days (see also Gillies et al., 2010a). As shown in Fig. 3, day-to-day increases in $PM_{2.5}$ occur as the multi-day episodes evolve. We compute typical rates of increase during these episodes in two ways. First, a mean rate of 9 μg m^{-3} d^{-1} from the onset to the peak

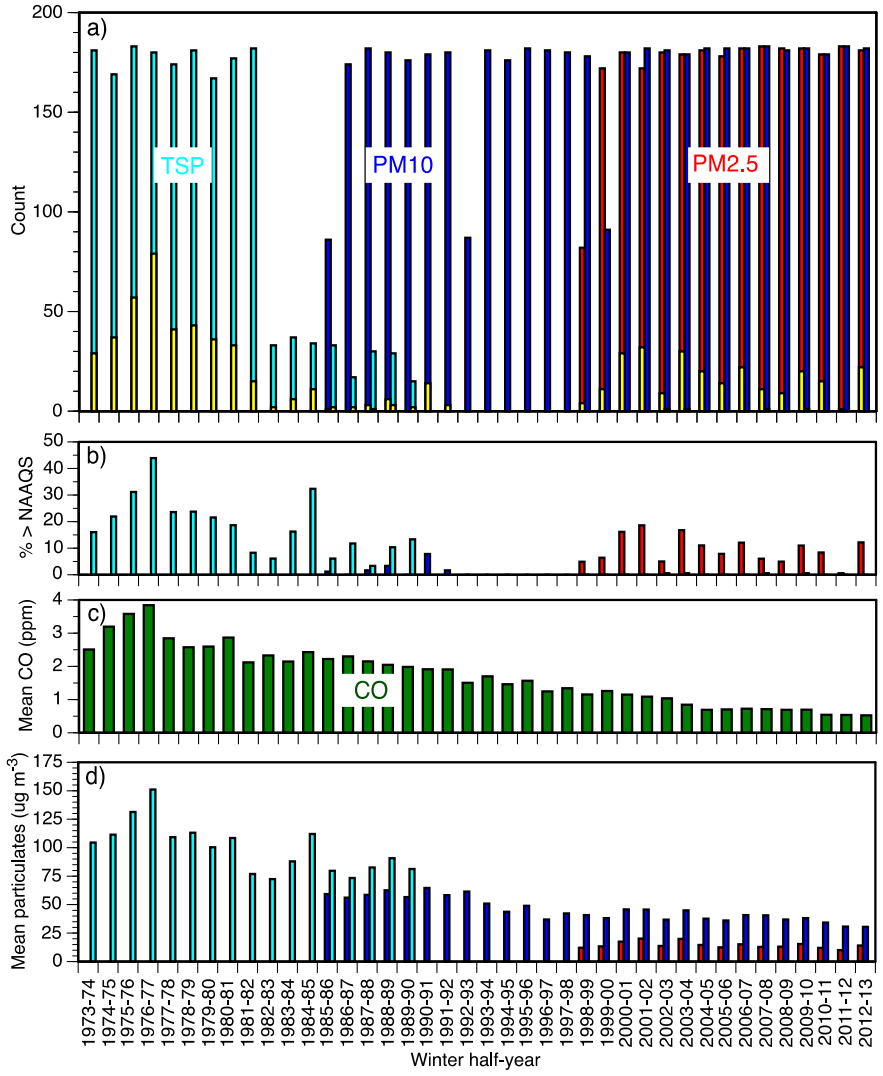

Fig. 6. a) Number of 24-h-average samples of TSP (cyan), PM_{10} (blue) and $PM_{2.5}$ (red) concentrations in the winter half-years. Yellow columns indicate the number of these samples exceeding the respective NAAQSes. b) Percentage of winter daily particulate measurements exceeding the NAAQS of 150 μg m^{-3} for TSP and PM10 and 35 μg m^{-3} for $PM_{2.5}$. c) Winter mean CO concentrations. d) Winter TSP, PM_{10} and $PM_{2.5}$ concentrations. There are 182 possible samples in most years, with 183 in leap years.

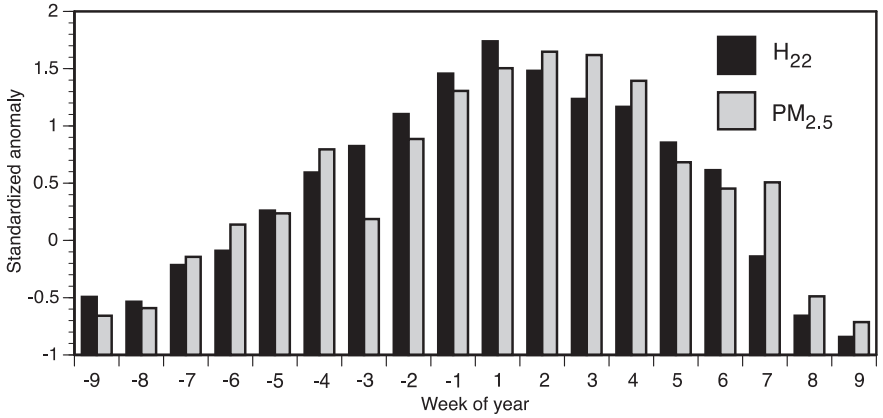

Fig. 7. Standardized anomalies of $PM_{2.5}$ and H_{22} by week of the year. Week 1 is 1–7 January, week −1 is 25–31 December, etc. The POR for twice-daily H_{22} is 1 Jan 1973 through 31 Mar 2013 and for daily $PM_{2.5}$ is 1 Jan 1999 through 31 Mar 2013.

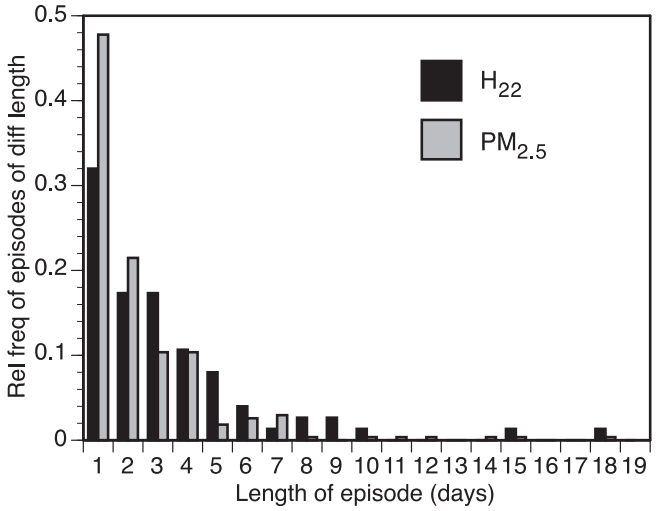

Fig. 8. Relative frequency of $PM_{2.5}$ > 35 μg m^{-3} and H_{22} > 4.04 MJ m^{-2} episodes of different lengths. $PM_{2.5}$ POR: 75 episodes, 1 Jan 1999 through 31 Mar 2013. H_{22} POR: 270 episodes, 1 Jan 1973 through 31 Mar 2013.

concentration is derived based on 49 episodes in the 1999 through 2011 period during which concentrations exceeded 35 μg m^{-3} for at least 3 days. Second, the $PM_{2.5}$ concentration is composited as a function of the day number of the multi-day episodes during which twice-daily H_{22} remained above 4.04 MJ m^{-2} for the entire 1999–2013 period (Fig. 9). According to Fig. 9, the rate of increase is 11 μg m^{-3} d^{-1} between the first sounding with H_{22} > 4.04 (day 0.5) and day 4. Daily average concentrations do not increase much beyond about 60 μg m^{-3} in long-lasting episodes.

3.2. Air quality–meteorology relationships

3.2.1. Valley heat deficit, H_{22}

Not surprisingly, H_{22} varies over a wide range of temporal scales. Returning to Fig. 5c, the monthly mean values of H_{22}, like those of $PM_{2.5}$, reach a maximum in mid-winter (3.59 MJ m^{-2} in January) and below 1.5 MJ m^{-2} in summer. The small, but positive, H_{22} values from spring to fall reflect the nighttime temperature inversions that are often present in the morning that are usually destroyed after sunrise by daytime convection. However, the afternoon soundings tend to have small positive values as the atmosphere generally is stable in the SLV with a sub-adiabatic lapse rate from the surface to the ridge top. Returning as well to Fig. 7, H_{22} standardized anomalies rise gradually during the fall and early winter to reach peak values around the beginning of the calendar year, earlier than the peak $PM_{2.5}$ values later in January.

The relative frequency of PCAP episodes in which H_{22} remained continuously above the 4.04 MJ m^{-2} threshold is shown in Fig. 8. To keep missing data from arbitrarily breaking a long episode into two shorter episodes, H_{22} values above the threshold were interpolated across short gaps that were missing one or two consecutive soundings (21 and 6 cases, respectively). Two hundred and seventy PCAP episodes occurred during the 40 winters, for an average of 6.8 episodes per winter. The mean length of the episodes was 6.2 soundings or 3.1 days. While PCAPs have persisted for up to 19 days, it is rather unusual for individual episodes to last longer than about 5 days. There are, however, many consecutive episodes that are separated by short interruptions as weak weather systems transit the valley and temporarily reduce atmospheric stability (Lareau and Horel, 2014a). 78% of the episodes began with a morning sounding and 68% ended following a morning sounding. Because traveling synoptic-scale disturbances and their effects on cold-air pools can be expected to be rather evenly distributed over the diurnal cycle, the high frequency of morning initiations and post-morning destructions indicates that local-scale processes play a significant role in the cold-pool buildup and breakup cycles.

The number of soundings with H_{22} > 4.04 MJ m^{-2} varied between 28 and 87 from winter to winter; that is, from 7.8 to 24.9% of the winter soundings (Fig. 10a). There are, on average, 60 soundings per year with H_{22} > 4.04 MJ m^{-2}. The winter-mean H_{22} varied from 1.80 MJ m^{-2} in 1977–1978 to 3.34 MJ m^{-2} in 1983–1984, with a mean value of 2.41 and standard deviation of 0.36 MJ m^{-2} (Fig. 10b). Thus, the record is characterized by large interannual variability. From Fig. 10, there is no statistically significant long-term trend in H_{22} over the 40-year winter record.

Large daily values of wintertime $PM_{2.5}$ are closely related to those of H_{22} (Fig. 3). On longer time scales, the year-to-year variations in winter mean values of $PM_{2.5}$ and H_{22} are strongly correlated for the relatively small sample of 15 winter seasons for which $PM_{2.5}$ values are available ($r = 0.83$, compare also the red boxes in Fig. 6d to Fig. 10b). This relationship does not account for year-to-year

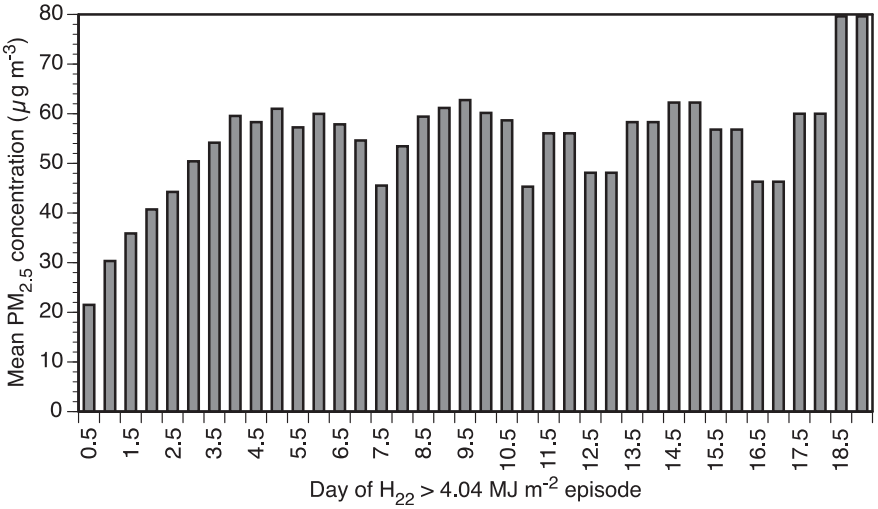

Fig. 9. Mean $PM_{2.5}$ concentration versus the day of a winter episode in which H_{22} remains above 4.04 MJ m^{-2}. Note from Fig. 8 the small number of cases after day 9. POR: 1 Jan 1999 through 31 Mar 2013.

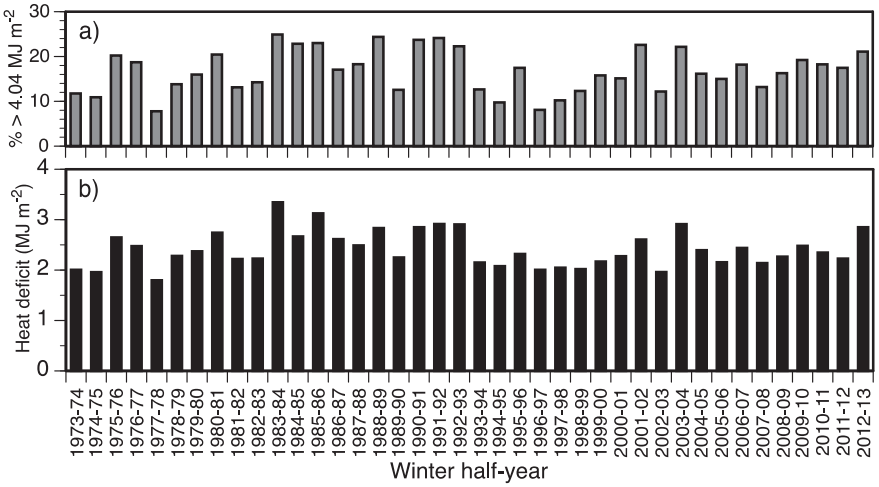

Fig. 10. a) Percentage of 12-hourly soundings for which H_{22} exceeds 4.04 MJ m^{-2}, and b) mean wintertime H_{22}.

changes in emission rates of reactants or primary particulates, or for other factors such as snow cover, cloud cover, winds, or humidity that play important roles in $PM_{2.5}$ production. Hence, the year-to-year H_{22} variations prior to 1999 may be reasonable proxies for earlier $PM_{2.5}$ variations, e.g., higher levels of $PM_{2.5}$ could be expected to have taken place in the early 1980s and 1990s.

PCAP events are usually initiated by a persistent large-scale, high-pressure center or ridge that transits the Intermountain Basin from west to east (Whiteman et al., 1999, 2001; Reeves and Stensrud, 2009; Zardi and Whiteman, 2012; Lareau et al., 2013). The geopotential height pattern progression leading to these events, as obtained by compositing 500 mb data from the North American Regional Reanalyses (Mesinger et al., 2006) for 97 PCAP episodes of differing length, is documented in the Supplemental Information. As the ridge approaches the SLV it brings warmer temperatures above the valley through warm air advection and synoptic-scale subsidence (Whiteman et al., 1999; Reeves and Stensrud, 2009). These large-scale events occur contemporaneously at multiple sites in the Intermountain Basin (Reeves and Stensrud, 2009). The increase in atmospheric stability caused by warm-air advection aloft is illustrated in Fig. 11. Atmospheric stability increases when the air warms above the valley without a corresponding increase in surface temperature. A succession of these warming events occurs throughout the winter separated by trough passages and/or cold fronts.

3.2.2. *Atmospheric conditions during $PM_{2.5}$ exceedance episodes*

Histograms of the wintertime relative frequencies of selected meteorological variables averaged over the surface-2200 m layer (the *valley column*) are shown for both daytime and nighttime soundings by the shaded boxes in Fig. 12. On days when $PM_{2.5} > 35\ \mu g\ m^{-3}$, averaged column temperatures tend to be below freezing (roughly 60% of time as shown in Fig. 12a) while relative humidity is nearly always greater than 50% (over 80% of the time as shown in Fig. 12b). Relative humidity varies inversely with temperature and increases as evaporation from the ground adds humidity to confined stable atmospheres.

Winds in mountain valleys are generally bi-directional, flowing up the valley during daytime and down the valley during nighttime, while in snow-covered valleys the winds predominantly blow down-valley (Whiteman, 2000). The SLV follows this pattern (Fig. 12c). Nighttime winds are more frequently from the south, while daytime winds are more frequently from the north. These diurnal wind shifts are not interrupted during NAAQS exceedances, i.e., the open boxes show similar directional dependencies. Wind speeds vary as winter storms associated with low-pressure centers alternate with light winds associated with high-pressure ridging. Low wind speeds are equally distributed between night (0500 MST) and day (1700 MST), but wind speeds above 5 m s^{-1} tend to occur preferentially at night. $PM_{2.5}$ exceedances occur with weaker than normal wind speeds. Roughly 60% of the time the valley column wind speed is less than 3 m s^{-1} (Fig. 12d). Surface pressure is higher than normal (Fig. 12e) and H_{22} is much higher than normal (Fig. 12f) during exceedances. Table 1 summarizes the small likelihood of having a $PM_{2.5}$ exceedance given H_{22} below the threshold (~3%) as well as the increased likelihood of having a $PM_{2.5}$ exceedance given H_{22} above the threshold (~42%, i.e., 7.6% divided by 18%). When a $PM_{2.5}$ exceedance is underway, H_{22} is above the threshold on 76% of the days.

Both snow cover and cloud cover are conducive to the formation of persistent multi-day inversions as they both reflect incoming solar radiation back to space and, thus, reduce the sensible heat flux at the ground that could produce growing unstable boundary layers that destroy atmospheric stability during daytime. At night snow cover is a good black body radiator and insulates the atmosphere from the generally warmer underlying ground, providing cooling needed to strengthen stable layers. Cloud cover at night, on the other hand, reduces nighttime cooling to space. Radiative interactions between the cloud base and ground destabilize the temperature structure and promote better mixing below cloud base. Morning fogs, often lifting later in the day to form low clouds, are often present during PCAPs. The moisture required to form the clouds can come from evaporation/sublimation, from up-valley advection from the nearby Great Salt Lake, or from precipitation falling into the PCAP from above.

Snow cover and cloud cover frequencies (Fig. 13) are highest during mid-winter when $PM_{2.5}$ exceedances are most likely. The probability of snow cover increases gradually in the last 7 weeks of the year, peaking in the second week of January and remaining high through mid-February, with a rapid decrease over the following several weeks. The probability of low stratus/stratocumulus or fog reaches a maximum in the next to last week of December and declines slowly thereafter. The relationships between $PM_{2.5}$ concentrations and snow cover are summarized in Table 2. There is snow on the ground at the airport on roughly 25% of the winter days. The probability of having $PM_{2.5}$ > NAAQS increases from 5.3% when there is no snow cover (4%/74.9%) to 22% when there is snow cover present (5.6%/25.1%), or roughly a 4-fold increase. When low

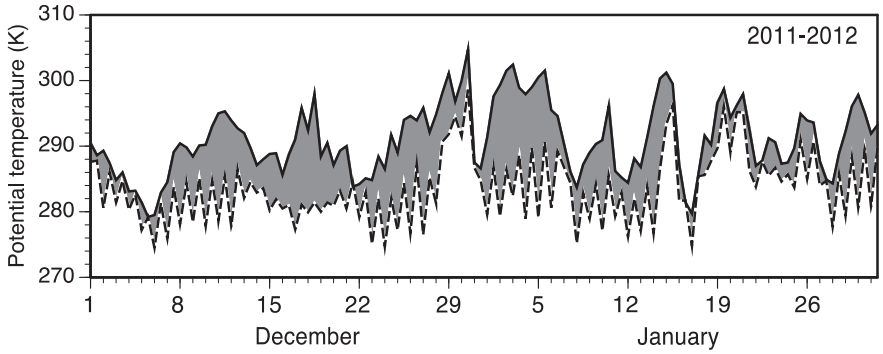

Fig. 11. Potential temperatures from 12-hourly rawinsonde ascents at KSLC for 2200 m MSL (solid line) and the surface (dashed line). The shading between the upper and lower curves is a measure of atmospheric stability in the valley.

clouds are present, there is a greater chance for exceedance conditions (44% vs. 9%), but the limited sample size of cloudy days precludes this association as being relevant (not shown). Additional categorical analyses show that if $H_{22} > 4.04$ MJ m^{-2}, $\overline{T}_{22} < 5$ °C, $\overline{r}_{22} > 60\%$ and snow cover is present, there is a 75% chance that $PM_{2.5}$ concentrations will exceed the NAAQS.

3.2.3. Interannual and intraseasonal relationships

Standardized anomalies on two distinct time scales were derived to compare: 1) filtered seasonal means of air quality and bulk stability variables, and 2) daily pollutant and meteorological variables within winter seasons. The intent in the first case is to reduce the effects of the pollutant control strategies that are evident in the seasonal means shown in Fig. 6. To do so, the nonlinear *4253H twice* median smoother (Tukey, 1977; Velleman, 1980, 1988) was applied to the time series of winter mean PM_{10}, $PM_{2.5}$ and H_{22}. The differences between each winter mean and the smoothed winter median for that winter were divided by the POR standard deviation of those differences for that variable. The resulting standardized anomaly time series are closely related to one another (Fig. 14), with a $PM_{2.5}$–PM_{10} correlation coefficient of 0.84, and a $PM_{2.5}$-H_{22} correlation coefficient of 0.93. Interestingly, $PM_{2.5}$-CO standardized anomalies are poorly correlated (−0.040) since CO has been controlled over time such that its long-term fluctuations do not relate to those found in the other variables. Gases and particulates can also be expected to have different residence times in the atmosphere.

To relate variations within the winter seasons in the meteorological fields to those of $PM_{2.5}$, the median values for each winter season are first subtracted from the daily values for each variable. This removes any year-to-year and longer-term trend signals from the analysis that can arise naturally as well as due to evolving control strategies. Standardized daily anomalies for each variable for each day are obtained by dividing the daily departures from the seasonal median by the standard deviation of those daily fluctuations about the median. The resulting correlations between $PM_{2.5}$ and other variables are shown for the winter half-year in Table 3. Because the stable layer in the valley traps all atmospheric emissions, $PM_{2.5}$ is well correlated with PM_{10} and CO. These correlations might be higher still if the measurements were made at the same site. The highest meteorological correlation is with H_{22}. This correlation is higher than with an alternate measure of stability $\theta_{22}-\theta_{sfc}$. Other high correlations are with the "day of the episode, *doe*".

The signs of the correlation coefficients indicate whether increases in the selected variable are associated with increases (+) or decreases (−) of $PM_{2.5}$ levels. $PM_{2.5}$ decreases with higher wind speeds in or at the top of the column, with higher Froude numbers, and with higher daily total solar radiation. Daily total solar radiation can be viewed as a seasonal timing variable with its minimum in late December when high values of $PM_{2.5}$ are common. Other variables whose increase is associated with increases in $PM_{2.5}$ are column humidity, column maximum humidity and snow depth.

A multiple linear regression was used to estimate the standardized daily anomalies of $PM_{2.5}$ concentrations by successively selecting variables in a stepwise fashion, choosing the variable best correlated with the regression residuals. The equation for $PM_{2.5}$ is:

$$\hat{y} = b_0 + \sum_{i=1}^{p} b_i x_i \tag{3}$$

where the variables used, x_i, and their coefficients, b_i, are given in Table 4.

Equation (3), with coefficients determined from daily winter data in the Jan 1999–Mar 2011 POR was used to estimate daily $PM_{2.5}$ values for the two following (independent) winters. The winter of 2011–2012 had only one and 2012–2013 had 21 daily $PM_{2.5}$ exceedances. This approach, however, is not predictive, as the analysis can only be made after the completion of each winter season. Furthermore, the association is between $PM_{2.5}$ concentrations and meteorological measurements *at the same time*. Thus, we are not using forecasts of the meteorological quantities. Estimated values are shown as a function of the observed values in Fig. 15. The Pearson product–moment correlation coefficient for the data pairs is $r = 0.67^{0.5} = 0.81$; the scatter demonstrates that this relatively strong apparent relationship depends on estimating low values of $PM_{2.5}$ well many times while doing a poorer job of estimating the less common episodes of anomalously high $PM_{2.5}$. Referring back to Table 1, the regression relationship tends to emphasize the strong associations in the upper left quadrant (low $PM_{2.5}$ and low H_{22}).

The stepwise multiple linear regression between meteorology and air pollution variables is marginally stronger when limited to December through February rather than the entire winter half-year, but the stepwise order of the independent variables changes (Table 4). Bulk stability, mean wind speed in the column, and snow cover continue to play important roles. Potential daily total solar radiation, however, adds little skill for the shorter period, and humidity variables play an enhanced role. The reduction of variance in $PM_{2.5}$ produced by the independent variables is approximately the same as for the entire winter season, despite the reduction by 50% in the number of cases in the regression.

4. Conclusions

Atmospheric particulate concentrations in Utah's topographically confined SLV have generally decreased over the last 40 years

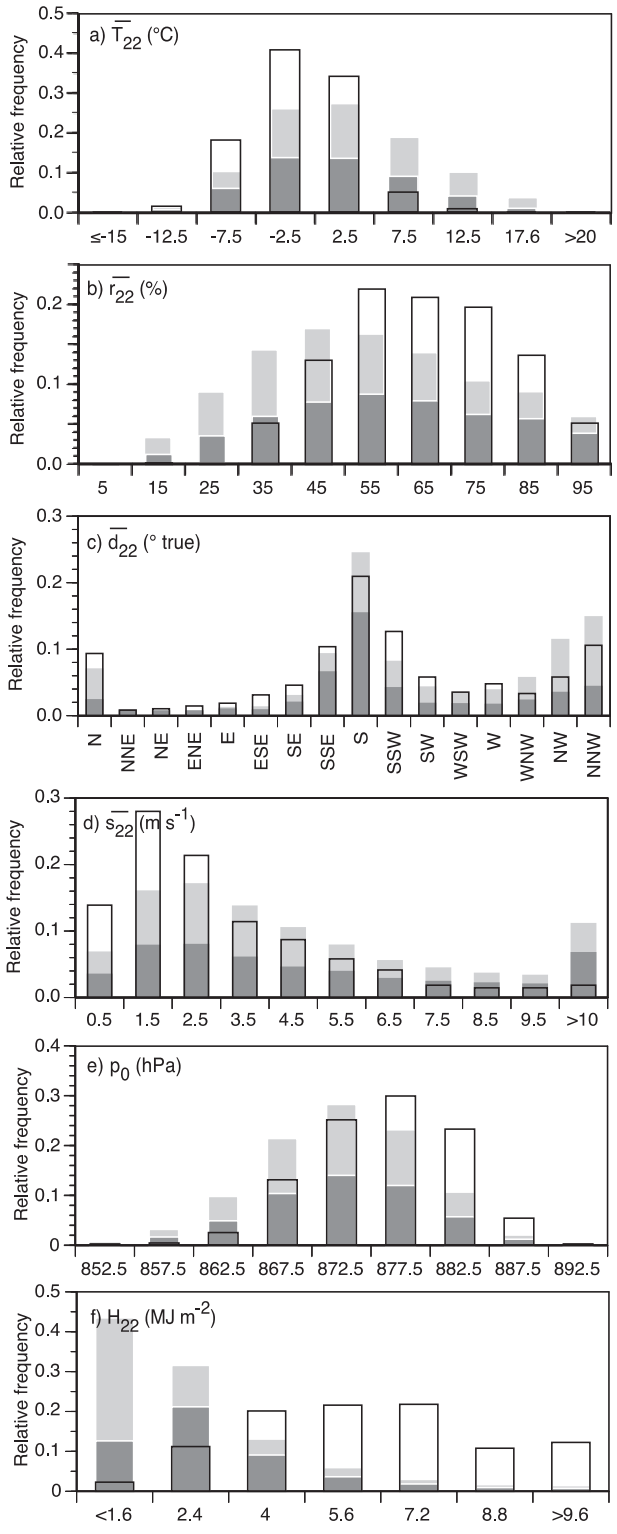

Fig. 12. Wintertime relative frequency of surface-to-2200 m MSL mean a) temperature, b) relative humidity, c) wind direction, and d) wind speed. e) is surface pressure and f) is heat deficit. The stacked shaded columns indicate the 0500 (dark gray) and 1700 MST (light gray) observations in the period 1 Jan 1973 to 31 Mar 2013. The top of this stack can be compared to the open boxes, which represent the relative frequencies for days with $PM_{2.5} > 35$ μg m^{-3} in the period 1 Jan 1999 through 31 Mar 2013. Categories are labeled by their midpoint. Bin sizes are 5 °C, 10%, 1 m s^{-1}, 22.5°, 5 hPa and 1.6 MJ m^{-2}, respectively.

Table 1
Contingency table for $PM_{2.5}$ and H_{22}. Cell values are % of 4830 total observations.

	$H_{22} \leq 4.04$	$H_{22} > 4.04$	Total
$PM_{2.5} \leq 17.5$ μg m^{-3}	69.1	4.0	73.1
$17.5 < PM_{2.5} \leq 35$ μg m^{-3}	10.5	6.4	16.9
$PM_{2.5} > 35$ μg m^{-3}	2.3	7.6	10.0
Total	82.0	18.0	100

as air quality regulations have taken effect. However, the SLV is presently exceeding the 2006 federal 24-h-average NAAQS for fine particulates in winter. The exceedances typically occur during multi-day high atmospheric stability episodes associated with high-pressure ridges that transit the Intermountain Basin. The 35 μg m^{-3} standard is exceeded approximately 18 days per winter, and the concentrations increase approximately 10 μg m^{-3} d^{-1} over the first 4–5 days of the episode before reaching a plateau. Concentrations on weekdays and weekends do not differ significantly.

Atmospheric factors play a major role in limiting dispersion in the SLV. Of special importance is the reduction of vertical dispersion occasioned by wintertime episodes of strong atmospheric stability. Pollution episodes are triggered by an elevated valley heat deficit, a vertically integrated measure of atmospheric stability. $PM_{2.5}$ exceedances are more likely to occur when snow cover is present; surface pressure and column-mean relative humidity are high; and column-mean temperatures and wind speeds are low. These meteorological factors are, no doubt, closely related to the atmospheric chemistry of the secondary particulates (Kroll and Seinfeld, 2008). Reflection from the snow cover produces enhanced levels of solar radiation for photochemical reactions and the high humidity and low temperatures are important for the deliquescence, formation and conservation of secondary particulates.

Our climatological analyses have focused largely on bulk or vertically integrated measures of meteorological variables. Perhaps the most surprising finding is that $PM_{2.5}$ concentrations measured at the valley floor were well correlated with heat deficits integrated to rather high altitudes in the valley, emphasizing the strong influence of synoptic- or large-scale meteorological controls on air pollution events. When the valley heat deficit is strong, vertical mixing is suppressed and winds within the valley become decoupled from the generally stronger winds aloft, allowing moisture, fogs, low clouds, pollutants and other scalars to build up within the stable air mass.

A 40-y climatology of particulate matter and meteorological variables in the SLV is used to investigate winter-to-winter relationships among air quality and meteorological variables after adjusting for long-term trends as regulations have been applied. $PM_{2.5}$ concentrations have decreased only modestly since 1999, with large meteorologically driven winter-to-winter variations in both the number of $PM_{2.5}$ exceedances and the mean concentrations. A close association between heat deficit and $PM_{2.5}$ concentrations on winter, weekly and daily time scales suggests that the long record of twice-daily heat deficits can be a proxy for particulate concentrations, extending the 14.5 year $PM_{2.5}$ record back in time. The statistical relationships for $PM_{2.5}$ are hampered by the relatively short period of measurements, by the use of daily average values that cannot resolve shorter-term weather changes, and by the fact that the valley heat deficit is a trigger variable in which a range of $PM_{2.5}$ concentrations can be associated with single heat deficit values.

No statistically significant long-term trend in wintertime atmospheric stability can be detected in the 40-y record. A stepwise multiple linear regression analysis shows that $PM_{2.5}$ concentrations are best estimated by the valley heat deficit, surface to 2200-m-

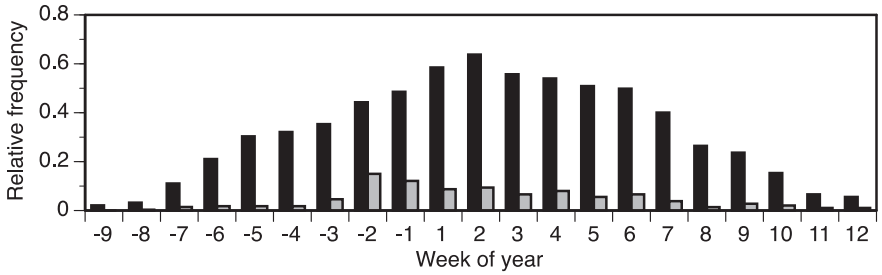

Fig. 13. Relative frequency of snow cover >0 cm (black) and low-cloud cover (gray) at KSLC in the daily reports of the week indicated. Week 1 is 1–7 January, week −1 is 25–31 December, etc.

Table 2
Contingency table for $PM_{2.5}$ and snow cover. Cell values are % of 5190 total observations.

	No snow cover	Snow cover	Total
$PM_{2.5} \leq 17.5$ μg m^{-3}	60.9	13.6	74.5
$17.5 < PM_{2.5} \leq 35$ μg m^{-3}	10.0	5.9	15.9
$PM_{2.5} > 35$ μg m^{-3}	4.0	5.6	9.6
Total	74.9	25.1	100

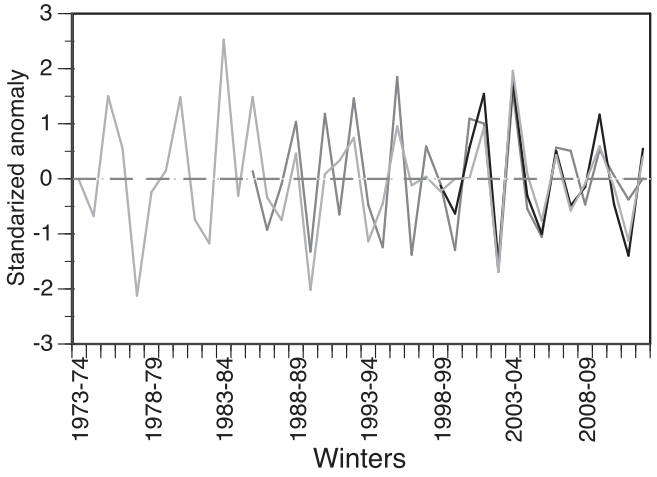

Fig. 14. Standardized anomalies of wintertime 24-h-mean H_{22} (light gray), PM_{10} (medium gray), and $PM_{2.5}$ (black) for 1973–74 through 2012–2013.

Table 3
Pearson product–moment correlations between daily standardized anomalies of $PM_{2.5}$ and other air quality and meteorological variables. Shown are variables for which the absolute value of the correlation coefficient exceeds 0.20.

x	Correlation coefficient
H_{22}	0.694
CO	0.646
PM_{10}	0.644
doe	0.632
$\theta_{22}-\theta_{sfc}$	0.571
rad	−0.413
p_{sfc}	0.339
F_1	−0.308
r_{max}	0.308
$\bar{s}_{22}$	−0.294
F_2	−0.290
sdepth	0.217

Table 4
Multiple linear regression independent variables, coefficients and cumulative adjusted r^2 for $PM_{2.5}$ (Eq. (3)). POR: winter months, 1 Jan 1999 through 31 Mar 2011.

i	Oct–Mar			Dec–Feb		
	x	*b*	r^2 (%)	*x*	*b*	r^2 (%)
0		−0.0204	0		−0.0069	0
1	H_{22}	0.5688	46.7	H_{22}	0.5736	48.0
2	$\bar{s}_{22}$	−0.2552	50.0	$\bar{s}_{22}$	−0.2533	53.4
3	*rad*	−0.1666	53.2	r_{max}	0.2592	53.9
4	*sdepth*	0.0675	53.6	*sdepth*	0.0536	54.2
5	F_1	0.1082	54.3	p_0	0.0465	54.3
6	r_{max}	0.2723	54.6	$\bar{r}_{22}$	−0.1837	54.9

average wind speed and humidity, theoretical daily total solar radiation and snow depth. An application of the regression equation to a 2-y independent data set resulted in a good correlation between actual and estimated daily $PM_{2.5}$ concentrations; however this strong relationship manifests most clearly as an association between the more common occurrences of low heat deficits and low values of $PM_{2.5}$.

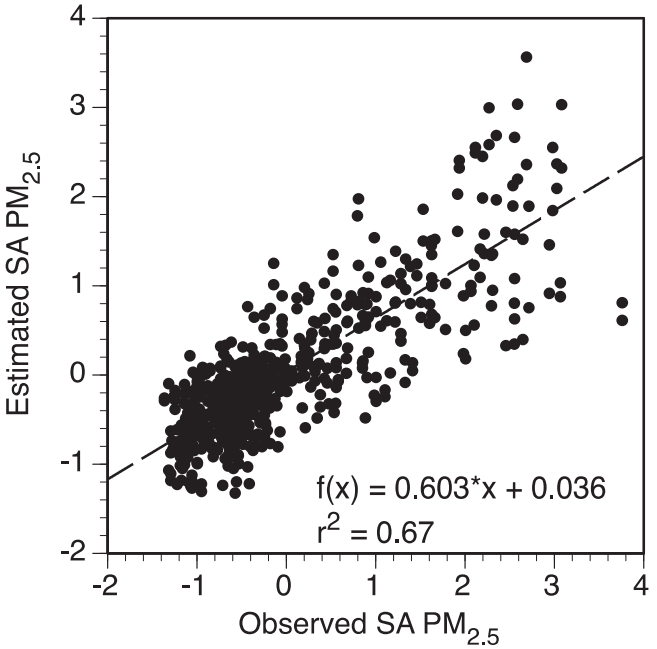

Fig. 15. Comparison of observed and predicted daily standardized anomalies of $PM_{2.5}$ for the winters of 2011–2012 and 2012–2013 using Eq. (3).

Acknowledgments

This research was supported by National Science Foundation grant ATM-0938397. The National Weather Service and UDAQ collected the rawinsonde and air quality data. Kimberley Kreykes and Lance Avey (UDAQ) provided supplementary air quality data and metadata. Neil Lareau produced Fig. 1.

Appendix A. Supplementary data

Supplementary data related to this article can be found at http://dx.doi.org/10.1016/j.atmosenv.2014.06.012.

References

Bailey, A., Chase, T.N., Cassano, J.J., Noone, D., 2011. Changing temperature inversion characteristics in the U. S. Southwest and relationships to large-scale weather circulations. J. Appl. Meteorol. Climatol. 50, 1307–1323.

Baker, K.R., Simon, H., Kelly, J.T., 2011. Challenges to modeling "cold pool" meteorology associated with high pollution episodes. Environ. Sci. Technol. 45, 7118–7119.

Beard, J.C., Beck, C., Graham, R., Packham, S.C., Traphagan, M., Giles, R.T., Morgan, J.G., 2012. Winter temperature inversions and emergency department visits for asthma in Salt Lake City, Utah, 2003–2008. Environ. Health Perspect. 120, 1385–1390.

Chen, L.-W.A., Watson, J.G., Chow, J.C., Green, M.C., Inouye, D., Dirk, K., 2012. Wintertime particulate pollution episodes in an urban valley of the Western US: a case study. Atmos. Chem. Phys. 12, 10051–10064.

Gillies, R.R., Wang, S.-Y., Booth, M.R., 2010a. Atmospheric scale interaction on wintertime Intermountain West low-level inversions. Weather Forecast. 25, 1196–1210.

Gillies, R.R., Wang, S.-Y., Yoon, J.-H., Weaver, S., 2010b. CFS prediction of winter persistent inversions in the Intermountain region. Weather Forecast. 25, 1211–1218.

Holzworth, G.C., Fisher, R.W., 1979. Climatological Summaries of the Lower Few Kilometers of Rawinsonde Observations. EPA-600/4-79-026, U.S. EPA. 141 pp. (Available from NTIS, Springfield, VA 22161).

Hosler, C.R., 1961. Low-level inversion frequency in the contiguous United States. Mon. Weather Rev. 89, 319–339.

International Organization for Standardization, 1975. Standard atmosphere. ISO 2533.

Kelly, K.E., Kotchenruther, R., Kuprov, R., Silcox, G.D., 2013. Receptor model source attributions for Utah's Salt Lake City airshed and the impacts of wintertime secondary ammonium nitrate and ammonium chloride aerosol. J. Air Waste Manag. Assoc. 63, 575–590.

Kroll, J., Seinfeld, J., 2008. Chemistry of secondary organic aerosol: formation and evolution of low-volatility organics in the atmosphere. Atmos. Environ. 42, 3593–3624.

Lareau, N., Crosman, E., Whiteman, C.D., Horel, J.D., Hoch, S.W., Brown, W.O.J., Horst, T.W., 2013. The persistent cold-air pool study. Bull. Am. Meteorol. Soc. 94, 51–63.

Lareau, N., Horel, J., 2014a. Dynamically induced displacements of a persistent cold-air pool. Bound. Layer. Meteorol. (in press).

Lareau, N. and J. Horel, 2014b: Turbulent erosion of cold-air pools. Submitted J. Atmos. Sci..

Leung, L.R., Gustafson, W.I., 2005. Potential regional climate change and implications to U.S. air quality. Geophys. Res. Lett. 32, L16711 http://dx.doi.org/10.1029/2005GL022911.

Lu, W., Zhong, S., 2014. A numerical study of a persistent cold air pool episode in the Salt Lake Valley, Utah. J. Geophys. Res. Atmos. 119, 1733–1752.

Malek, E., Davis, T., Martin, R.S., Silva, P.J., 2006. Meteorological and environmental aspects of one of the worst national air pollution episodes (January, 2004) in Logan, Cache Valley, Utah, USA. Atmos. Res. 79, 108–122.

Mesinger, F., et al., 2006. North American Regional Reanalysis. Bull. Am. Meteorol. Soc. 87, 343–360.

Mickley, L.J., Jacob, D.J., Field, B.D., Rind, D., 2004. Effects of future climate change on regional air pollution episodes in the United States. Geophys. Res. Lett. 31, L24103 http://dx.doi.org/10.1029/2004GL021216.

Milionis, A.E., Davies, T.D., 2008. The effect of the prevailing weather on the statistics of atmospheric temperature inversions. Int. J. Climatol. 28, 1385–1397.

Peters, A., Liu, E., Verrier, R.L., Schwartz, J., Gold, D.R., Mittleman, M., Baliff, J., Oh, J.A., Allen, G., Monahan, K., Dockery, D.W., 2000. Air pollution and incidence of cardiac arrhythmia. Epidemiology 11, 11–17.

Pope, C.A., Dockery, D.W., Spengler, J.D., Raizenne, M.E., 1991. Respiratory health and PM_{10} pollution. A daily time series analysis. Am. Rev. Respir. Dis. 144, 668–674 http://dx.doi.org/10.1164/ajrccm/144.3_Pt_1.668.

Pope III, C.A., Muhlestein, J.B., May, H.T., Renlund, D.G., Anderson, J.L., Horne, B.D., 2006. Ischemic heart disease events triggered by short-term exposure to fine particulate air pollution. Circulation 114, 2443–2448.

Reeves, H.D., Stensrud, D.J., 2009. Synoptic-scale flow and valley cold pool evolution in the western United States. Weather Forecast. 24, 1625–1639.

Silcox, G.D., Kelly, K.E., Crosman, E.T., Whiteman, C.D., Allen, B.L., 2012. Wintertime $PM_{2.5}$ concentrations in Utah's Salt Lake Valley during persistent, multi-day cold-air pools. Atmos. Environ. 46, 17–24.

Smith, R., Paegle, J., Clark, T., Cotton, W., Durran, D., Forbes, G., Marwitz, J., Mass, C., McGinley, J., Pan, H.-L., Ralph, M., 1997. Local and remote effects of mountains on weather: research needs and opportunities. Bull. Am. Meteorol. Soc. 78, 877–892.

Tukey, J.W., 1977. Exploratory Data Analysis. Addison-Wesley, Reading, MA.

Utah Division of Air Quality, 2013. Utah State Implementation Plan: Control Measures for Area and Point Sources, Fine Particulate Matter, $PM_{2.5}$ SIP for the Salt Lake City, Ut. Nonattainment Area, 4 Dec 2013. (online, cited 4 Mar 2014). http://www.airquality.utah.gov/Pollutants/ParticulateMatter/PM25/SIPImp/docs/2013/12Dec/SIPIX.A.21_Adopted_12-4-13.pdf.

Velleman, P.F., 1988. Data Desk Version 6 Statistics Guide. Data Description, Inc., Ithaca, New York.

Velleman, P.F., 1980. Definition and comparison of robust nonlinear smoothing algorithms. J. Am. Stat. Assoc. 75 (371), 609–615.

Whiteman, C.D., Bian, X., Zhong, S., 1999. Wintertime evolution of the temperature inversion in the Colorado Plateau Basin. J. Appl. Meteorol. 38, 1103–1117.

Whiteman, C.D., 2000. Mountain Meteorology: Fundamentals and Applications. Oxford University Press, New York, p. 355.

Whiteman, C.D., Zhong, S., Shaw, W.J., Hubbe, J.M., Bian, X., Mittelstadt, J., 2001. Cold pools in the Columbia Basin. Weather Forecast. 16, 432–447.

Wolyn, P.G., McKee, T.B., 1989. Deep stable layers in the intermountain Western United States. Mon. Weather Rev. 117, 461–472.

Young, J.S., 2013. Investigation of Wintertime Cold-air Pools and Aerosol Layers in the Salt Lake Valley Using a Lidar Ceilometer. M. S. Thesis. Department of Atmospheric Sciences, University of Utah, p. 106.

Zardi, D., Whiteman, C.D., 2012. Diurnal mountain wind systems. Chapter 2. In: Chow, F. K., S. F. J. DeWekker, B. Snyder (Eds.), Mountain Weather Research and Forecasting. Springer, Berlin, pp. 35–119.

Zhong, S., Xu, X., Bian, X., Lu, W., 2011. Climatology of persistent deep stable layers in Utah's Salt Lake Valley, USA. Adv. Sci. Res. 6, 59–62.